Angular dependence and phase diagrams of exchange-coupled epitaxial $Ni_{81}Fe_{19}/Fe_{50}Mn_{50}(001)$ bilayers

T. Mewes, H. Nembach, M. Rickart, S. O. Demokritov, J. Fassbender, and B. Hillebrands
Fachbereich Physik and Forschungs- und Entwicklungsschwerpunkt Materialwissenschaften, Universität Kaiserslautern, D-67663 Kaiserslautern, Germany
(Received 7 January 2002; revised manuscript received 8 April 2002; published 7 June 2002)

The exchange bias effect, especially the angular dependence of the exchange bias field and the coercivity of the epitaxial $Ni_{81}Fe_{19}/Fe_{50}Mn_{50}$ bilayer system is investigated. In order to prepare a well defined layer sequence large emphasis is laid on the structural characterization of each layer. Low-energy electron diffraction and scanning tunneling microscopy are employed after each deposition step and the height-height-correlation function is analyzed to quantify the interface quality. Successively the angular dependence of the longitudinal and transverse magnetic component is investigated by magneto-optic Kerr effect magnetometry. In order to fully analyze the magnetization reversal behavior a special gray scale representation of the data is chosen. Theoretical results based on a modified Stoner-Wohlfarth model, which includes unidirectional and fourfold anisotropy contributions, are presented and compared to the experimental results. Although a homogeneous rotation of the magnetization is assumed the agreement between theory and experiment is surprisingly good. Only in a narrow angular range, where an ongoing rotation of the magnetization is predicted by the Stoner-Wohlfarth theory, discrepancies arise. The angular dependence of the possible orientations of the magnetization are summarized in a phase diagram.

DOI: 10.1103/PhysRevB.65.224423 PACS number(s): 75.70.−i, 75.30.Gw, 75.60.Jk, 75.40.Mg

I. INTRODUCTION

The exchange coupling between a ferromagnetic and an antiferromagnetic material[1,2] manifests itself, in addition to many other effects, in a shift of the magnetization loop away from zero-field by a value referred to as the exchange bias field H_{EB}, i.e., in an unidirectional anisotropy. This effect has received much attention in recent years because of its technological importance in magnetoresistive sensors and read heads as well as for magnetic random access memory.[3,4] But still today, more than forty years after the discovery of this effect, its microscopic origin has not yet been completely understood. The first model proposed by Meiklejohn and Bean[1,2] predicts an exchange bias field which is two orders of magnitude larger than observed experimentally. The random-field model by Malozemoff[5,6] and the model by Mauri *et al.*,[7] which proposes a planar domain wall in the antiferromagnet, both account for this discrepancy. These models, as well as others in the literature have achieved variable degree of agreement with different specific properties observed experimentally in exchange bias systems. However there is no comprehensive theory describing the exchange bias effect. For recent reviews concerning both theory and experiment see Refs. 8–10.

Since the exchange bias effect is an interfacial effect the structure of the interface between the ferromagnetic and antiferromagnetic layer is of great importance. In the case of polycrystalline layered systems the situation is further complicated due to the spread in grain orientation. In order to gain a deeper understanding of the underlying microscopic origin of the exchange bias effect well characterized epitaxial layered systems are required. Recently measurements of the magnetization reversal of both polycrystalline and epitaxial exchange bias systems as a function of the in-plane angle of the applied field with respect to the unidirectional anisotropy direction have been reported.[11–15] It has been recognized that the resulting angular dependence of the exchange bias field and the coercivity can be well described including higher order anisotropy contributions in the Stoner-Wohlfarth model.[16] The aim of this paper is to provide a detailed picture of angular dependence of the whole magnetization reversal process for epitaxial $Ni_{81}Fe_{19}/Fe_{50}Mn_{50}(001)$ bilayers. We propose a new scheme to visualize the large amount of experimental data allowing for an easier access to the information contained. The general features of the magnetization reversal behavior are well described within a modified Stoner-Wohlfarth model including an unidirectional and a fourfold anisotropy term. We discuss corresponding phase diagrams.

II. EXPERIMENT

The samples were prepared in an UHV system with a base pressure of 5×10^{-11} mbar. In order to deposit epitaxial NiFe/FeMn bilayers on commercially available single crystalline MgO(001) substrates, a buffer layer system consisting of Fe(0.5 nm)/Pt(5 nm)/Cu(100 nm) is used with the Fe and Pt seed layers to induce the (001) orientation of the Cu buffer layer. The preparation conditions and the structural characterization of this buffer layer system is reported elsewhere.[17] The samples consists of a 5 nm thick NiFe layer and a 10 nm thick FeMn layer, and they were covered with 2 nm Cu and 1.5 nm Cr to prevent them from oxidation. The different materials were evaporated either from Knudsen cells (Cu, Mn) or using *e*-beam evaporators (Fe, Pt, NiFe, Cr) with deposition rates typically between 0.01 and 0.1 nm/s. The surface cleanliness and chemical composition were checked using Auger spectroscopy. The sample morphology and its crystal quality was investigated *in situ* by means of low-

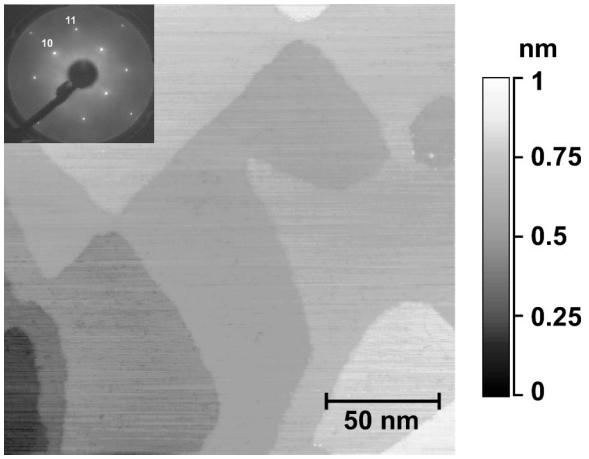

FIG. 1. STM image of MgO/Fe(0.5 nm)/Pt(5 nm)/Cu(100 nm), the scan area is 0.2 μm$\times$0.2 μm and the full height scale is 1 nm. The inset shows the corresponding LEED pattern for a primary energy of 165 eV.

energy electron diffraction (LEED), reflection high-energy diffraction (RHEED), and scanning tunneling microscopy (STM). After preparation the samples were briefly annealed in UHV slightly above the Néel-Temperature of bulk FeMn (500 K) while a magnetic field of 500 Oe was applied along an in-plane [110] direction of NiFe. The magnetic properties were measured *ex situ* at room temperature by using a magneto-optical Kerr effect (MOKE) magnetometer, probing both the longitudinal and the transverse component of the magnetization.

III. RESULTS

A. Structural properties

As described in the preceding section, a Cu(001) buffer layer is prepared to serve as a growth template with a large lateral correlation length, a low RMS-roughness and a small mosaicity suitable for the growth of NiFe.[17] The quality of this buffer layer is further improved by a careful anneal at 900 K. A STM-image of the resulting Cu(001) surface is shown in Fig. 1. Large, atomically flat terraces are separated by monoatomic steps running preferentially along the $\langle 110 \rangle$ directions. In order to quantify the STM images the height-height correlation function $H(\mathbf{r}) = \langle [h(\mathbf{r}) - h(\mathbf{0})]^2 \rangle$ has been determined using a procedure described in Ref. 18. Here $h(\mathbf{r})$ is the surface height at position $\mathbf{r}$ of the surface. For a self-affine and isotropic surface $H(r)$ can be expressed as $H(r) = 2w^2\{1 - \exp[-(r/\xi)^{2\alpha}]\}$, where α is the roughness exponent describing the texture of roughness, ξ is the lateral correlation length defining a typical lateral size of the roughness pattern, and w is the interface width [root-mean square (RMS) roughness].[19] The corresponding RMS roughness of the 0.2 μm$\times$0.2 μm scan area shown in Fig. 1 is 0.14 nm. The roughness exponent α was determined from larger STM images as $\alpha = 0.7 \pm 0.1$, which corresponds to a smooth sur-

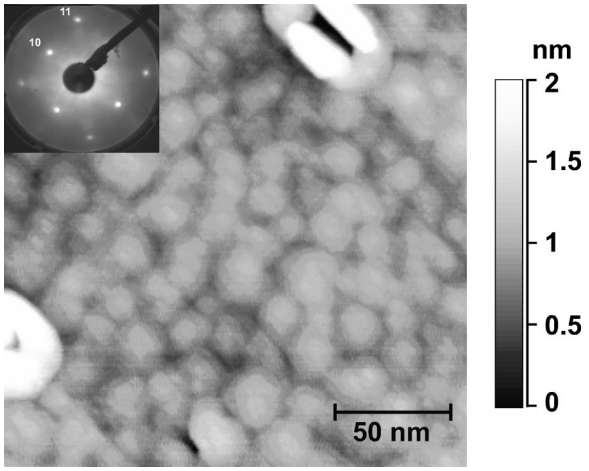

FIG. 2. STM image of MgO/Fe(0.5 nm)/Pt(5 nm)/Cu(100 nm)/NiFe(5 nm); the scan area is 0.2 μm$\times$0.2 μm and the full height scale is 2 nm. The inset shows the corresponding LEED pattern for a primary energy of 112 eV.

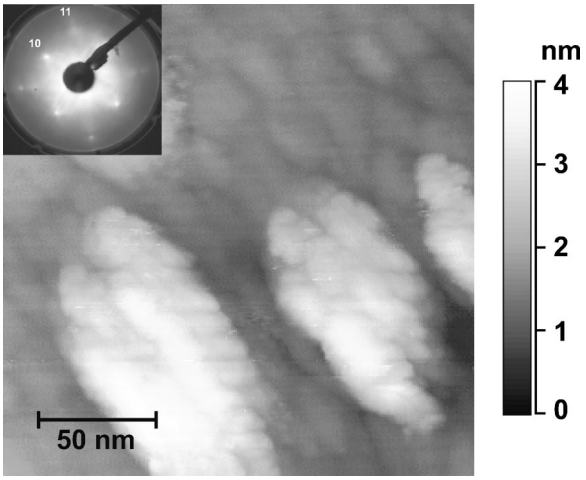

FIG. 3. STM image of MgO/Fe(0.5 nm)/Pt(5 nm)/Cu(100 nm)/NiFe(5 nm)/FeMn(10 nm); the scan area is 0.2 μm$\times$0.2 μm and the full height scale is 4 nm. The inset shows the corresponding LEED pattern for a primary energy of 115 eV.

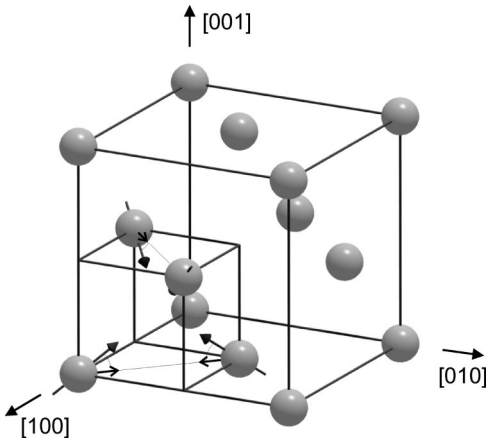

FIG. 4. Three-dimensional spin structure of FeMn according to the $\langle 111 \rangle$ model. The projection of the spin directions onto the (001) surface are also indicated by black arrows.

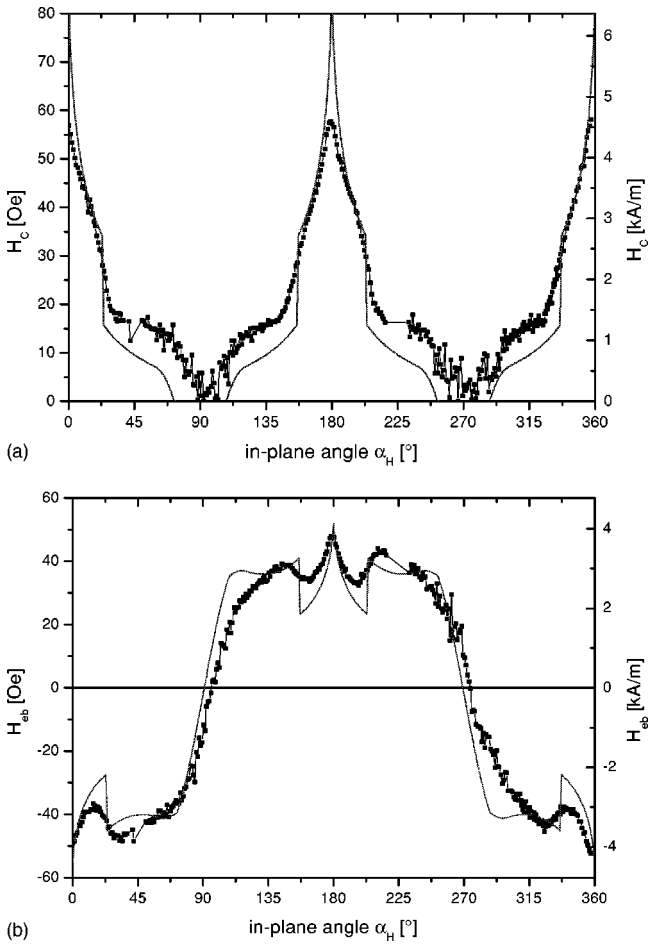

FIG. 5. Angular dependencies of the coercivity H_C (a) and of the exchange bias field H_{EB} (b) as derived from MOKE measurements. In both plots the measured values (symbols) and fit curves obtained using a free energy expression with unidirectional and fourfold anisotropy constants (lines) are shown.

face. Even for the largest possible scan area of 1 μm $\times 1$ μm the correlation length ξ is beyond the scan size. The corresponding LEED image exhibits narrow spots (see inset of Fig. 1). A 5 nm thick NiFe layer was subsequently deposited at 370 K. The quality of the corresponding LEED spots is slightly reduced but indicates still a good crystallographic structure of the surface (see inset of Fig. 2). The surface investigated by STM (see Fig. 2) mainly consists of small islands. This fact is also reflected in a small correlation length $\xi = 25$ nm. The RMS roughness of the 0.2 μm $\times 0.2$ μm scan area shown in Fig. 2 is 0.3 nm. The small value of the roughness exponent $\alpha = 0.5 \pm 0.1$ determined from larger STM images is caused by the relatively jagged surface of NiFe. In addition characteristic volcanolike features, also referred to as ''pinholes,'' are observed in Fig. 2, similar to those observed for the growth of Co on Cu(001).[20] The most commonly used explanation for the creation of these ''pinholes'' rely on surface and interface energies since formation of pinholes can result in a reduction of surface and interface energies.[20,21] Subsequently the FeMn layer is deposited at 370 K. The STM image shown in Fig. 3 shows a rather rough surface. The RMS roughness for a 0.2 μm $\times 0.2$ μm scan area of this 10 nm thick FeMn layer is 0.7 nm, which is larger than that of the NiFe layer. The correlation length $\xi = 50 \pm 5$ nm as well as the roughness exponent $\alpha = 0.6 \pm 0.1$ are also increased compared to the NiFe surface, i.e., the surface of FeMn has a larger RMS roughness but is less jagged and consists of larger islands than its interface with NiFe. Therefore special caution has to be taken when the properties of interfaces are extrapolated from the properties of the corresponding surfaces of layered systems. Nevertheless a good crystallographic structure is evidenced by the LEED pattern shown in the inset of Fig. 3.

B. Magnetic properties

Before presenting the experimental results of the magnetic properties we consider the spin structure of FeMn and discuss the resulting implications for the model which will be used to describe the experimental data. According to the $\langle 111 \rangle$ model (also referred to as the 3 Q state of fcc FeMn), the projection of the easy axis directions of FeMn onto the (001) surface are the $\langle 110 \rangle$ directions,[22–25] as indicated in Fig. 4. Therefore the effective free energy density of the ferromagnetic layer resulting from the interaction with FeMn is assumed to consist of an unidirectional and a fourfold contribution only:

$$f = -K_1 \cos(\alpha_M) + K_4 \sin^2(\alpha_M)\cos^2(\alpha_M). \qquad (1)$$

Here α_M denotes the angle of the magnetization with respect to the easy axis of the unidirectional anisotropy, i.e., the [110] direction of NiFe, whereas K_1 and K_4 are the unidirectional and fourfold anisotropy constants, respectively. Note that in many systems an uniaxial anisotropy contribution to the free energy is found[12–14] which may have its origin in an intrinsic twofold symmetry of the interface or symmetry breaking caused by induced stress and magnetostriction. In the present system it is not necessary to include such a contribution. The free energy given in Eq. (1) is used within the Stoner-Wohlfarth model[16] to calculate the magnetization reversal. Furthermore it is assumed that the magnetization direction remains in a local minimum of the free enthalpy as long as the minimum exists. This is the so-called perfect delay convention.[26] By using this assumption the possibility of lowering the free enthalpy of the system by nucleation of reversed domains and propagation of domain walls in the ferromagnet is completely neglected. This is justified in exchange bias systems, where the mobility of domains is low due to the interaction with the antiferromagnet.[27] Furthermore thermal activation to overcome the involved energy barriers is also neglected. Thus the perfect delay convention predicts an upper limit for the coercivity. In contrast, the use of the so called Maxwell convention, which assumes that the magnetization directions always reflects the global minimum of the free enthalpy of the system, would result in magnetization reversal without hysteretic behavior and thus without coercivity.

Next the experimental results of the magnetization reversal behavior will be presented. From MOKE measurements in longitudinal geometry the coercive fields for the decreasing and increasing field branch $H_{C,\mathrm{left}}$ and $H_{C,\mathrm{right}}$, respec-

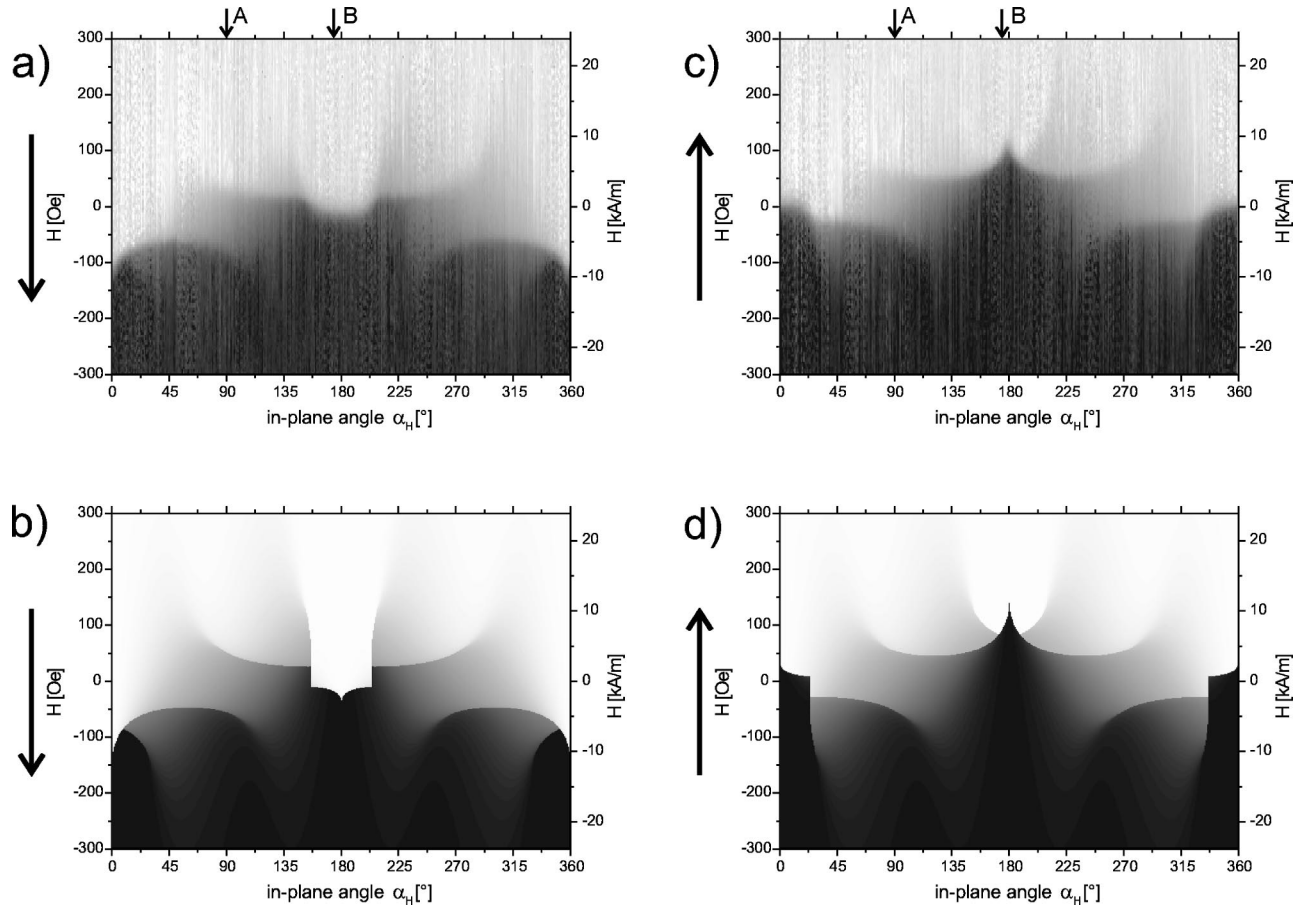

FIG. 6. Angular dependence of the longitudinal component of the magnetization for decreasing [(a) and (b)] and increasing field branch [(c) and (d)] of the hysteresis loop obtained experimentally [(a) and (c)] and theoretically within the Stoner-Wohlfarth model [(b) and (d)]. A detailed description of these magnetization reversal diagrams is given in the main text.

tively, are deduced. By varying the in-plane angle α_H of the applied field H with respect to the [110]-direction of NiFe the angular dependence of the coercive field $H_C(\alpha_H) = [H_{C,\mathrm{right}}(\alpha_H) - H_{C,\mathrm{left}}(\alpha_H)]/2$ and the exchange bias field $H_{EB}(\alpha_H) = [H_{C,\mathrm{right}}(\alpha_H) + H_{C,\mathrm{left}}(\alpha_H)]/2$ are derived. The obtained results are shown in Fig. 5 together with fit curves calculated using the free energy density given by Eq. (1) within the Stoner-Wohlfarth model with the perfect delay convention. The fitted constants are $K_1 = 4.6 \times 10^4$ erg/cm^3 and $K_4 = 3.8 \times 10^4$ erg/cm^3. Thus the easy axes of the unidirectional and fourfold anisotropy coincide with the [110] direction ($\alpha_M = 0$) and the anisotropy constants have the same order of magnitude. Notice that due to the fact that the perfect delay convention gives an upper limit for the coercivity the determined anisotropy constants have to be regarded as lower limits.

In order to compare not only the quantities H_C and H_{EB} which only rely on two points, namely, $H_{C,\mathrm{left}}$ and $H_{C,\mathrm{right}}$, of the hysteresis curve we present the whole data set for the longitudinal component of the magnetization in Figs. 6(a) and 6(c) in the following way: for both branches of the hysteresis curve, i.e., decreasing and increasing field branch, a gray-scale image is constructed. The gray level of each point is chosen to be proportional to the magnitude of the magnetization component parallel to H, in particular a point is set white (black) if the magnetization points exactly along the positive (negative) field direction. The horizontal cartesian coordinate of the point represents α_H whereas the vertical one represents the magnitude of H. To further illustrate this kind of data representation the magnetization reversal curves for the in-plane angles marked by the arrows A and B in Figs. 6(a) and 6(c) are shown in Fig. 7 in the conventional way, together with the gray scale used and the predictions of the Stoner-Wohlfarth model. The angular dependencies predicted by the Stoner-Wohlfarth model using the perfect delay convention are shown in Figs. 6(b) and 6(d) as a gray scale image as well. By comparing Fig. 6(a) with 6(b) and Fig. 6(c) with 6(d) it is obvious that the overall angular dependence of the longitudinal component of the magnetization during magnetization reversal is very well described by Eq. (1). In order to complete the picture of the magnetization reversal behavior the transverse magnetization component has been measured in additional MOKE measurements. In Fig. 8 the results are presented in a similar manner as in Fig. 6 but now the gray level is proportional to the magnitude of the magnetization component perpendicular to the applied field. By comparing the experimental results [Figs. 8(a) and 8(c)] with those of the corresponding theoretical prediction [Figs. 8(b) and 8(d)] it can be concluded that also the overall angular dependence of the transverse component of the mag-

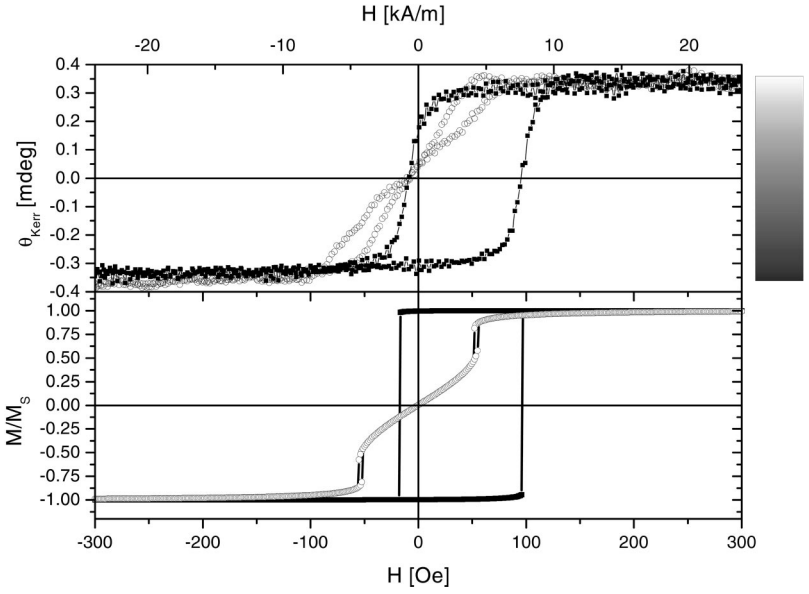

FIG. 7. Longitudinal component of the magnetization during magnetization reversal obtained experimentally by longitudinal MOKE measurements (upper panel) and calculated using the Stoner-Wohlfarth model (lower panel) . Two hysteresis curves are shown for $\alpha_H = 90°$ (open symbols) and $\alpha_H = 175°$ (closed symbols).

netization during magnetization reversal is correctly described within the Stoner-Wohlfarth model. There are two main differences that appear between experiment and the predictions of the Stoner-Wohlfarth model. (i) Sharp edges occurring in the Stoner-Wohlfarth model are somewhat rounded in the experiment. (ii) The peaklike structure present in the decreasing (increasing) field branch at 180° (0°), that appears in Figs. 6(b) and 8(b) [Figs. 6(d) and 8(d)] is not observed in the experiment as can be seen in Figs. 6(a) and 8(a) [Figs. 6(c) and 8(c)]. Interestingly enough this deviation

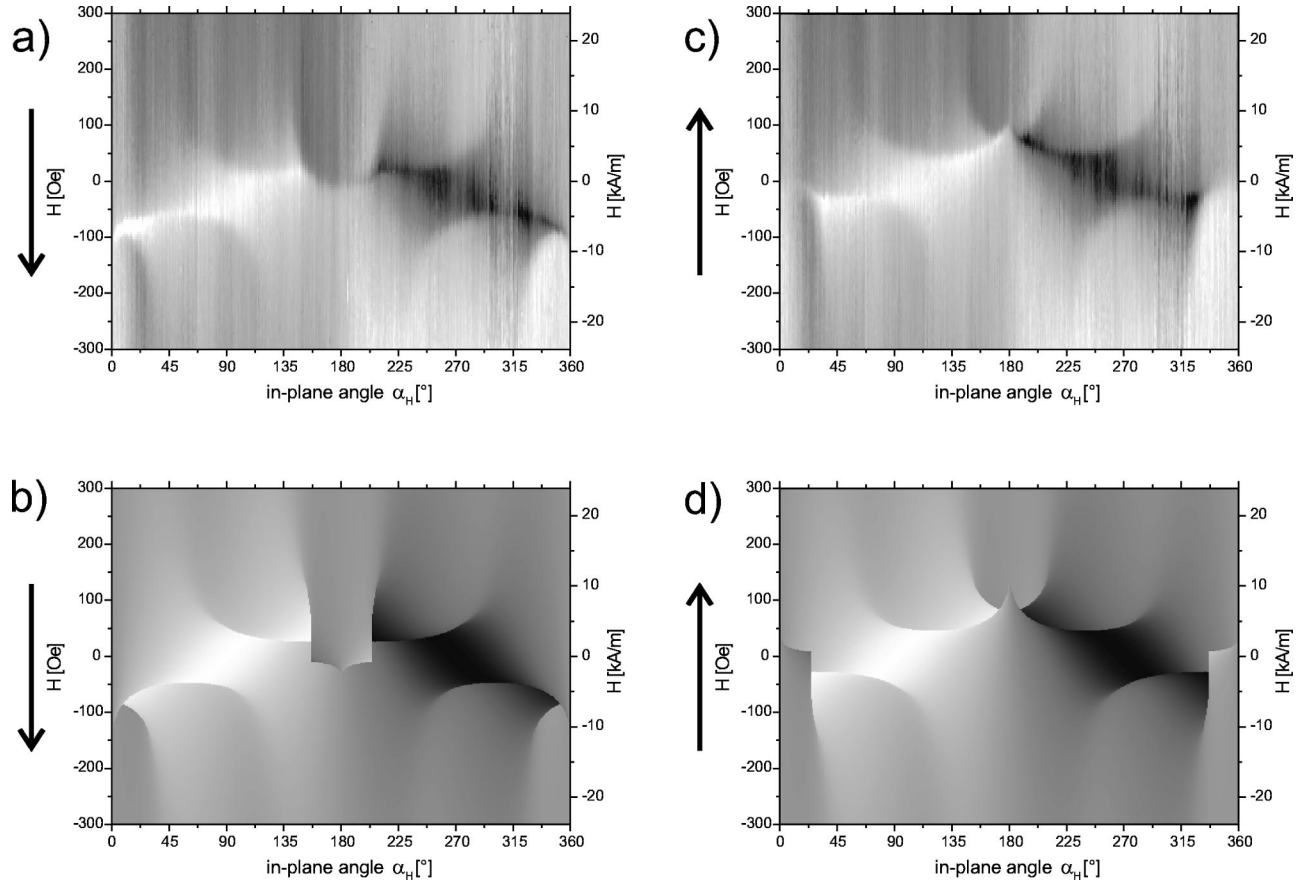

FIG. 8. Angular dependence of the transverse component of the magnetization for decreasing [(a) and (b)] and increasing field branch [(c) and (d)] of the hysteresis loop obtained experimentally [(a) and (c)] and theoretically within the Stoner-Wohlfarth model [(b) and (d)]. The data representation corresponds to that of Fig. 6, but the transverse magnetization magnitude is displayed in a gray level.

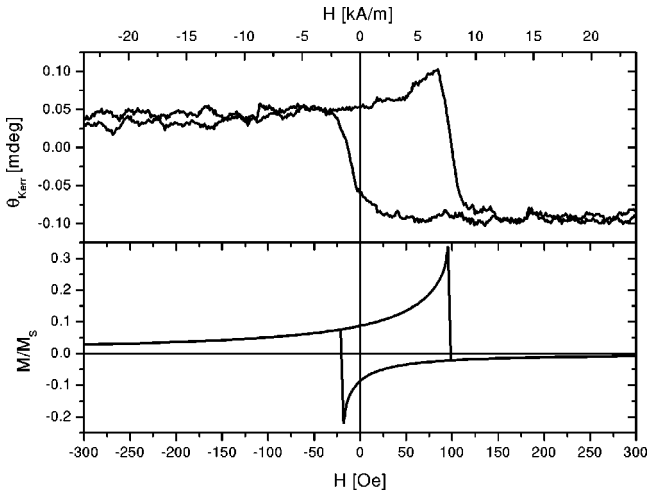

FIG. 9. Transverse component of the magnetization during magnetization reversal obtained experimentally by MOKE measurements (upper panel) and calculated using the Stoner-Wohlfarth model (lower panel). The in-plane angle of the applied magnetic field is in both cases $\alpha_H = 175°$.

appears in a narrow angular range at about $180° \pm 20°$ and $0° \pm 20°$ for which the Stoner-Wohlfarth model predicts a magnetization reversal for which the sense of rotation is the same for increasing and decreasing field branch, i.e., the magnetization rotates by 360° during a complete hysteresis loop. This kind of behavior was not observed in the experiment, as illustrated in Fig. 9. The measured transverse magnetization component and the one predicted by the Stoner-Wohlfarth model are shown for $\alpha_H = 175°$. This in turn shows that the Stoner-Wohlfarth model describes the general behavior quite well but cannot account for all features observed in exchange-biased bilayers. In addition to the possibility of domain formation and thermal activation to overcome the involved energy barriers, which are both neglected in the Stoner-Wohlfarth model, one other possible mechanism that prevents the magnetization from performing an ongoing rotation during magnetization reversal is the formation of a partial domain wall in the antiferromagnetic layer parallel to the interface.[7,28,29] However the ratio of the observed interface energy $\Delta E = K_1 t_{\mathrm{FM}} \approx 0.023$ erg/cm^2 (with $t_{\mathrm{FM}} = 5$ nm being the thickness of the NiFe layer) and the energy of a domain-wall in FeMn is, according to Ref. 7, well below the threshold for the domain-wall formation in the antiferromagnet. On the other hand, it has been shown recently that a twist in an antiferromagnetic FeMn layer between a NiFe and a Co layer exists.[30] Due to the tiny energy difference that determines the sense of rotation, it seems possible that even a small twist in the antiferromagnet can prevent the ferromagnet from performing an ongoing rotation. For further comparison between experiment and the different models we suggest to extend the model calculations to describe the vector of the magnetization during the magnetization reversal. A presentation in a similar form like the one given in Figs. 6 and 8 then enables a direct comparison between the models and experiment.

The angular dependence given in Figs. 6 and 8 is summarized in a phase diagram displayed in Fig. 10(a). This repre-

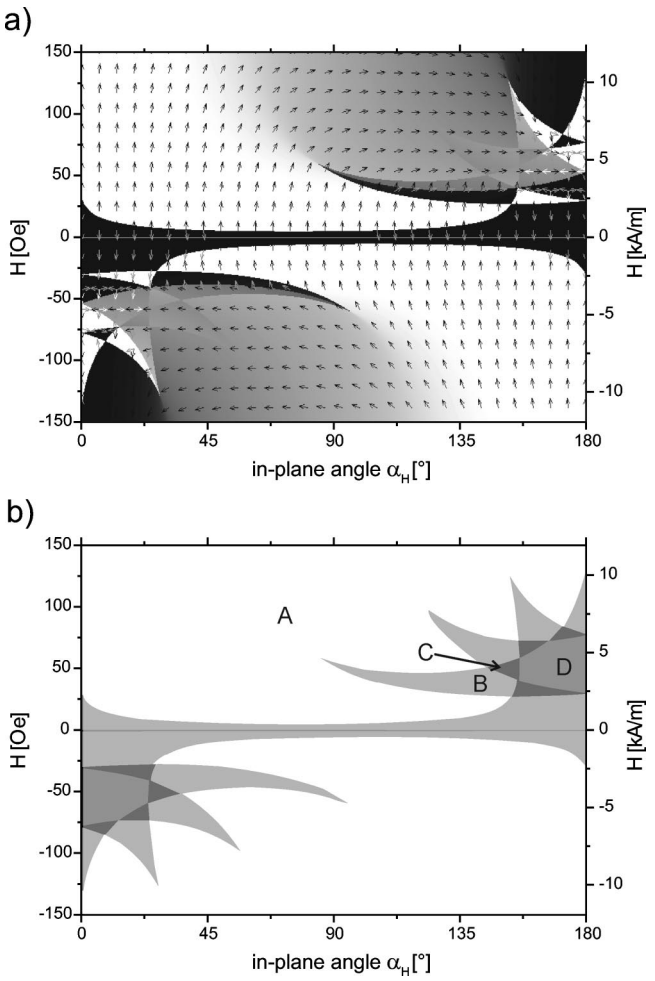

FIG. 10. Phase diagram for a system with unidirectional and four fold anisotropy contribution ($K_1 = 4.6 \times 10^4$ erg/cm^3 and $K_4 = 3.8 \times 10^4$ erg/cm^3) to the free enthalpy. The arrows in (a) indicate the direction of the magnetization in the minima of the free enthalpy. In (b) the regions for which there exist one, two, three, or four minima are labeled A, B, C, and D, respectively.

sentation is similar to the phase diagrams discussed for uniaxial ferromagnets[31,32] but focussed on the angular dependence. In the phase diagram shown in Fig. 10(a) the gray level is proportional to the angle $\alpha_{M,\mathrm{min}}$ between the magnetization direction and the easy axis (i.e., the [110] direction of NiFe) in the global minimum of the free enthalpy. In order to better distinguish between the different regions of the phase diagram where one, two, three, or even four minima exist in the free enthalpy the gray level is chosen as follows: For an odd number of minima white corresponds to $\alpha_{M,\mathrm{min}} = 0°$ and black corresponds to $\alpha_{M,\mathrm{min}} = 180°$, for an even number of minima it is just the opposite, white corresponds to $\alpha_{M,\mathrm{min}} = 180°$ and black to $\alpha_{M,\mathrm{min}} = 0°$. The regions with different numbers of minima are also sketched in the schematic phase diagram in Fig. 10(b), where different gray levels are used for these regions. The regions are labeled A, B, C, and D accordingly. The magnetization direction in the global minimum together with the directions for all other minima of the free enthalpy are furthermore indicated by small arrows in Fig. 10(a). The gray level of the arrows is

chosen according to the free enthalpy of the corresponding minima, i.e., a black arrow indicates the minimum of the magnetization direction with the lowest free enthalpy whereas a white arrow indicates the minimum with the highest free enthalpy. By comparing the angular dependence of the longitudinal and transverse components of the magnetization during reversal (Figs. 6 and 8) with the phase diagram given in Fig. 10 the crucial role of the phase boundaries separating the regions with different numbers of minima of the free enthalpy becomes obvious.

IV. CONCLUSIONS

In this paper the angular dependence of the exchange bias field and the coercivity as well as the complete magnetization reversal for the exchange coupled $Ni_{81}Fe_{19}/Fe_{50}Mn_{50}$ bilayer system epitaxially grown on MgO(001)/Fe/Pt/Cu have been studied experimentally. The overall angular dependence can be theoretically described within a modified Stoner-Wohlfarth model including an unidirectional and fourfold anisotropy with the same order of magnitude. Small differences between experiment and theoretical description appear for angles for which the Stoner-Wohlfarth model predicts an ongoing rotation of the magnetization during the hysteresis loop. The developed two-dimensional representation of the experimental data helps to systematically understand the magnetic properties.

ACKNOWLEDGMENTS

We would like to thank R.L. Stamps, J.V. Kim, and R. Lopusnik for stimulating and helpful discussions. One of the authors (T.M.) acknowledges suport by the Studienstiftung des deutschen Volkes.

[1] W.H. Meiklejohn and C.P. Bean, Phys. Rev. **102**, 1413 (1956).
[2] W.H. Meiklejohn and C.P. Bean, Phys. Rev. **105**, 904 (1957).
[3] J.M. Daughton, A.V. Pohm, R.T. Fayfield, and C.H. Smith, J. Phys. D **32**, R169 (1999).
[4] S.S.P. Parkin, K.P. Roche, M.G. Samant, P.M. Rice, R.B. Beyers, R.E. Scheuerlein, E.J. O'Sullivan, J. Bucchigano, D.W. Abraham, Y. Lu, M. Rooks, P.L. Trouilloud, R.A. Wanner, and W.J. Gallagher, J. Appl. Phys. **85**, 5828 (1999).
[5] A.P. Malozemoff, Phys. Rev. B **35**, 3679 (1987).
[6] A.P. Malozemoff, Phys. Rev. B **37**, 7673 (1988).
[7] D. Mauri, H.C. Siegmann, P.S. Bagus, and E. Kay, J. Appl. Phys. **62**, 3047 (1987).
[8] J. Nogues and I.K. Schuller, J. Magn. Magn. Mater. **192**, 203 (1999).
[9] A.E. Berkowitz and K. Takano, J. Magn. Magn. Mater. **200**, 552 (1999).
[10] R.L. Stamps, J. Phys. D **33**, R247 (2000).
[11] T. Ambrose, R.L. Sommer, and C.L. Chien, Phys. Rev. B **56**, 83 (1997).
[12] S. Riedling, M. Bauer, C. Mathieu, B. Hillebrands, R. Jungblut, J. Kohlhepp, and A. Reinders, J. Appl. Phys. **85**, 6648 (1999).
[13] H. Xi and R.M. White, J. Appl. Phys. **86**, 5169 (1999).
[14] Y.J. Tang, B.F.P. Roos, T. Mewes, M. Bauer, S.O. Demokritov, B. Hillebrands, and W.S. Zhan, Mater. Sci. Eng., B **76**, 59 (2000).
[15] C. Liu, J. Du, J.A. Barnard, and G.J. Mankey, J. Vac. Sci. Technol. A **19**, 1213 (2001).
[16] E.C. Stoner and E.P. Wohlfarth, Philos. Trans. R. Soc. London, Ser. A **240**, 599 (1948).
[17] T. Mewes, M. Rickart, A. Mougin, S.O. Demokritov, J. Fassbender, B. Hillebrands, and M. Scheib, Surf. Sci. **481**, 87 (2001).
[18] H.-N. Yang, Y.-P. Zhao, A. Chan, T.-M. Lu, and G.-C. Wang, Phys. Rev. B **56**, 4224 (1997).
[19] S.K. Sinha, E.B. Sirota, S. Garoff, and H.B. Stanley, Phys. Rev. B **38**, 2297 (1988).
[20] A.K. Schmid, D. Atlan, H. Itoh, B. Heinrich, T. Ichinokawa, and J. Kirschner, Phys. Rev. B **48**, 2855 (1993).
[21] R.T. Tung, Mater. Chem. Phys. **32**, 107 (1992).
[22] H. Umebayashi and Y. Ishikawa, J. Phys. Soc. Jpn. **21**, 1281 (1966).
[23] Y. Endoh and Y. Ishikawa, J. Phys. Soc. Jpn. **30**, 1614 (1971).
[24] R. Jungblut, R. Coehoorn, M.T. Johnson, C. Sauer, P.J. van der Zaag, A.R. Ball, T.G.S. Rijks, J. aan de Stegge, and A. Reinders, J. Magn. Magn. Mater. **148**, 300 (1995).
[25] T.C. Schulthess, W.H. Butler, G.M. Stocks, S. Maat, and G.J. Mankey, J. Appl. Phys. **85**, 4842 (1999).
[26] S. Nieber and H. Kronmueller, Phys. Status Solidi B **165**, 503 (1991).
[27] J.P. King, J.N. Chapman, M.F. Gillies, and J.C.S. Kools, J. Phys. D **34**, 528 (2001).
[28] M.D. Stiles and R.D. McMichael, Phys. Rev. B **59**, 3722 (1999).
[29] J. Geshev, Phys. Rev. B **62**, 5627 (2000).
[30] F.Y. Yang and C.L. Chien, Phys. Rev. Lett. **85**, 2597 (2000).
[31] Y.T. Millev, H.P. Oepen, and J. Kirschner, Phys. Rev. B **57**, 5837 (1998).
[32] Y.T. Millev, H.P. Oepen, and J. Kirschner, Phys. Rev. B **57**, 5848 (1998).